CHAPTER 6

PAPER-BASED SERS SUBSTRATE FOR THE DETECTION AND ANALYSIS OF ROTAVIRUS PARTICLES

This chapter illustrates a low-cost and sensitive SERS substrate developed on a printing-grade paper to detect rotavirus in clinical stool samples. The proposed SERS substrate has been fabricated through drop-casting AgNPs on a printing-grade paper. Rotavirus samples were extracted from clinical stool samples. The presence of rotavirus antigen in stool samples was confirmed using enzyme-linked immunosorbant assay (ELISA), polymerase chain reaction (PCR), and sequencing. The charateristic Raman peaks of rotavirus particles in solution have been found to be significantly enhanced when Raman signals were recorded from the paper-based SERS substrates.

6.1 Introduction

Rotavirus is one of the main causes of severe gastroenteritis in infants and children worldwide, leading to a high number of hospitalizations and deaths [1, 2]. Rotavirus infection still poses a hazard in low-income nations, although vaccination has decreased the number of fatalities linked to rotavirus illness in recent years [3, 4]. Recently, a new report on the spread of group B rotavirus in foals has been a concern for public and disease control authorities [5]. Thus, it is required to regularly monitor the spread of rotaviruses and prevent any possible future pandemic. Rotaviruses are non-enveloped double-stranded RNA viruses belonging to the family *Reoviridae*. Among the structural proteins (VP1, VP2, VP3, VP4, VP6, and VP7) rotavirus particles, VP4 and VP7 in the outer layer are used for serotyping and are crucial for vaccine development [2, 6]. Commonly used virus detection and identification techniques are PCR, sequencing-based tests, ELISA, and cell culture. However, the instruments required for these techniques are very expensive and bulky with time-consuming and

complicated sample preparation steps making these techniques unsuitable for rapid applications. RT-PCR [7, 8] and ELISA [9] are the most common techniques used to detect rotavirus. Researchers have used several alternative techniques to detect and identify rotaviruses. Using functionalized plasmonic label-free nanosensors based on a LSPR sensing platform, a rotavirus concentration of less than 10^3 plaque-forming units per mL (PFU mL^{-1}) has been detected [10]. Functionalizing the surface with anti-rotavirus antibodies, photonic crystal biosensors have been utilized in the label-free detection and rapid of porcine rotavirus [11]. Colloidal gold immunochromatographic assay (ICA) test strip has been designed to detect bovine rotavirus by utilizing the principle of the double-antibody sandwich method [12].

SERS technique has been utilized in the detection and identification of viruses, such as Influenza [13], SARS-CoV-2 [14], Hepatitis B [15], and HIV 1 [16]. With AgNR array SERS substrate, Driskell et al. have detected and identified different genotypes of rotavirus [17]. Using bio-conjugated hybrid graphene oxide-based SERS substrate, Fan et al. selectively removed rotavirus particles from the solution and detected prominent bands of the rotavirus sample [18]. SERS ICA has been developed using Raman molecule-labelled gold-silver core-shell nanoparticles for quantitative and rapid detection of rotavirus in feces [19].

Paper-based SERS substrates are cost-effective, flexible, biodegradable, and have the potential for mass production in ordinary laboratory conditions [20, 21]. Various techniques, including adsorption, self-assembly, brushing, inkjet printing, and in-situ synthesis, have been used to integrate the plasmonic metal nanoparticles with paper fibers [22, 23]. The uniform distribution of these nanoparticles and the creation of hot-spots are both influenced by the natural folds and fibre structures in the paper [24]. In this chapter, AgNPs were drop-casted on printing-grade paper to develop a sensitive and low-cost paper-based SERS substrate. Clinical stool samples were collected, and the presence of rotavirus particles was initially confirmed by VP6-based ELISA and PCR techniques. Upon confirming the presence of the rotavirus particles, Raman signal analysis has been performed using the designed SERS substrate. The performance of the suggested SERS substrates was investigated using various printing-grade papers, and it was discovered that the SERS substrate developed using 85 grams per square meter (GSM) paper delivers higher sensitivity than the other grade paper substrates. Figure 6.1(a) represents the schematic representation of the fabrication process of paper SERS substrates for the present work, while figure 6.1(b) represents the pictorial depiction of SERS signals being collected from the rotavirus sample.

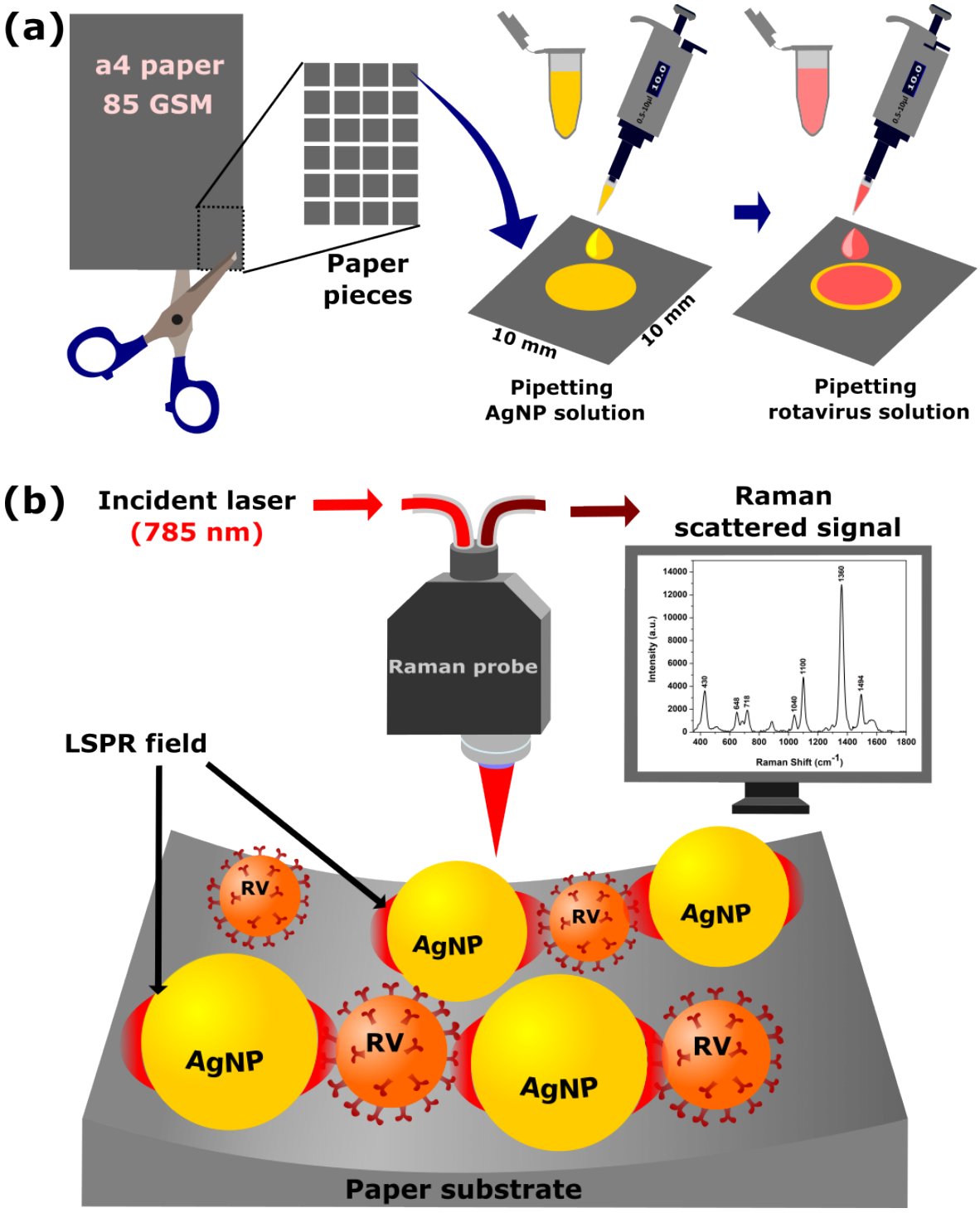

Figure 6.1: (a) Schematic representation of the fabrication process of the AgNP decorated paper-based SERS substrate, (b) Pictorial depiction of SERS signal collection from rotavirus samples adsorbed on a paper-based SERS substrate.

6.2 Materials and methods

6.2.1 Materials

Trisodium citrate dihydrate ($C_6H_5Na_3O_7{\cdot}2H_2O$) and silver nitrate ($AgNO_3$) were purchased from Merck, India. Raman active molecules, rhodamine 6G ($C_{28}H_{31}ClN_2O_3$) and malachite green ($C_{23}H_{25}ClN_2$) were procured from Alpha Aecer, India. 85 GSM and 100 GSM printing-grade papers were purchased from a local stationary shop. All chemicals were utilized as supplied without additional processing and deionized (DI) water was employed to prepare all experimental samples.

6.2.2 SERS substrate fabrication process

Colloidal AgNPs required for the proposed SERS substrate have been synthesized following the procedure discussed in the section 4.2.2 of Chapter 4. TEM image of the synthesized AgNPs is shown in the figure 6.2(a). The nanoparticles are mostly spherical and a very few have rod-like structure. Figure 6.2(b) depicts the histogram plot of the size distribution of the synthesized AgNPs calculated from the figure 6.2(a) using ImageJ software. Crystallinity of the AgNPs are measured from the selected area electron diffraction (SAED) pattern of the AgNP depicted in the figure 6.2(c). The concentric circular rings in the figure correspond to the lattice planes (111), (200), (220) and (311) of face centred cubic (fcc) silver [25]. Figure 6.2(d) shows the UV-Visible absorption spectrum of the synthesized AgNPs with a peak at 422 nm.

To fabricate the SERS substrates, two different printing-grade papers namely, 85 GSM and 100 GSM papers have been considered for the present study. These papers were cut into several small pieces of dimension 10 mm $\times$ 10 mm as depicted in the figure 6.1. The synthesized AgNP solution has been centrifuged at 3000 rpm for 10 minutes and 10 µL volume of the solution has been drop-casted on each of the paper substrates. These AgNP-treated paper pieces were then placed in a vacuum desiccator for 2 hour for drying. Figure 6.3(a) represents the photo image of AgNP decorated 85 GSM and 100 GSM paper SERS substrates. Surface morphologies of 85 GSM and 100 GSM paper SERS substrates captured by FESEM instrument are shown in figure 6.3(b) and 6.3(c), respectively. Figure 6.3(d) depicts the zoomed-in image of one AgNP cluster on 85 GSM paper SERS substrate. The fabricated substrates were then used for SERS-based sensing applications.

6.2.3 COMSOL simulation for the fabricated SERS substrates

Prior to the detection of Raman signals scattered from the proposed SERS substrate, the magnitudes of the LSPR field generated due to the coupling of the incident electro-

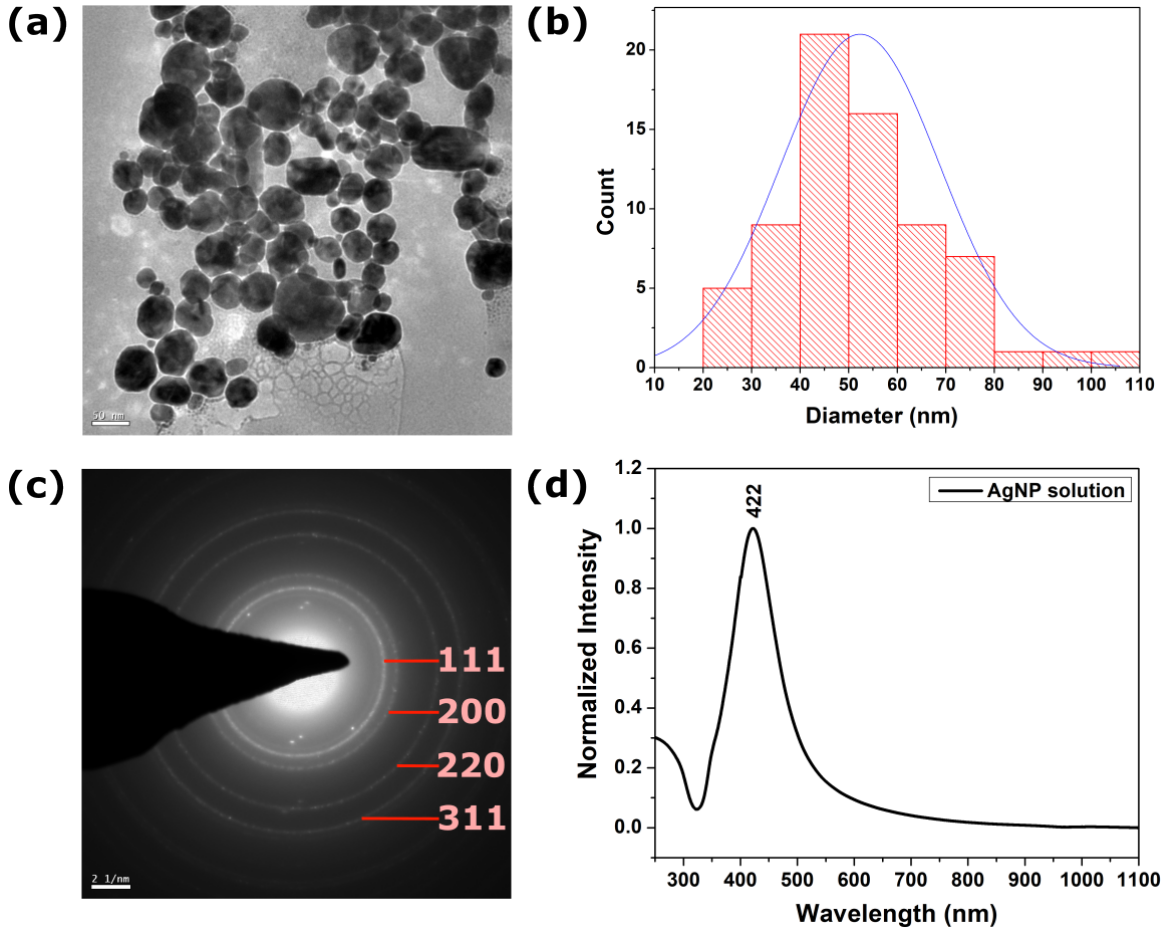

Figure 6.2: Characterization of synthesized AgNPs displaying the (a) TEM image with scale bar 50 nm. (b) Histogram of the diameter distribution of the AgNPs. (c) Electron diffraction pattern of the synthesized AgNPs in TEM. (d) UV-visible absorption spectrum with a peak at 422 nm.

magnetic fields with AgNP clusters has been studied using the Wave Optics Module of the COMSOL Multiphysics software. In this present simulation work, a 785 nm laser signal is allowed to interact with different distributions of AgNPs as displayed in figure 6.3(d). Estimation of the average LSPR field magnitude generated by the AgNPs is done by considering two indicated regions. Figure 6.3(e) and 6.3(f) represent the simulation results of the coupled electromagnetic field magnitudes for the considered regions. For both regions, the maximum field magnitudes of the order of $\sim 10^7$ Vm^{-1} has been observed which is equivalent to the maximum EF (EF_{max}) of $\sim 2 \times 10^6$. These simulation results suggest that the proposed AgNP decorated SERS substrate would be suitable for Raman signal analysis from the samples in trace concentrations.

6.2.4 Rotavirus extraction from stool samples and confirmation through ELISA and PCR

For the extraction of rotavirus from stool samples, we followed the protocol reported elsewhere [26, 27]. 30% viral suspension has been prepared by diluting the fecal samples with sterile 1X phosphate-buffered saline (PBS). The sample has been homogenized by vortex-mixing at room temperature followed by centrifugation at 12000 rpm for 10 minutes. The supernatants has been filtered through a 0.22 µm filter and 20%, 10% and 1% viral suspensions have been prepared by serial dilation. The detection of the rotavirus particles in the stool specimen have been performed using Premier Rotaclone® solid-phase sandwich enzyme immunoassay (EIA) that utilizes rotavirus VP6-specific monoclonal antibodies. In the assay displayed in figure 6.4(a), the colourless substrate is turned into yellow colour by the enzymes bound in the wells and the colour intensity is directly proportional to the concentration of the rotavirus antigen in the sample. Visual determinations have been made after 10 minutes of incubation with the ELISA substrates. Positive samples are those in which the yellow colour changes more than the negative control sample, while negative samples are those in which the colour change is less than or equal to the negative control sample. Spectrophotometric determinations have been carried out by adding 2 drops of 100 µL of Stop Solution (sulfuric acid) to each well after the incubation with substrates. A long-pass reference filter has been used to measure each well's absorbance at 450 nm. Absorbance less than 0.15 has been considered negative, while greater than or equal to 0.15 has been considered positive for the rotavirus.

The presence of other enteric viruses (adenovirus, astrovirus, norovirus) for all the samples has been confirmed by PCR using virus gene-specific primers followed by agarose gel electrophoresis and sequencing. The presence of rotavirus has been further confirmed by amplifying the VP7 gene which produces an amplicon of length 881 bp as shown in figure 6.4(b). CerTest Rota+Adeno+Astro+Noro, which is based

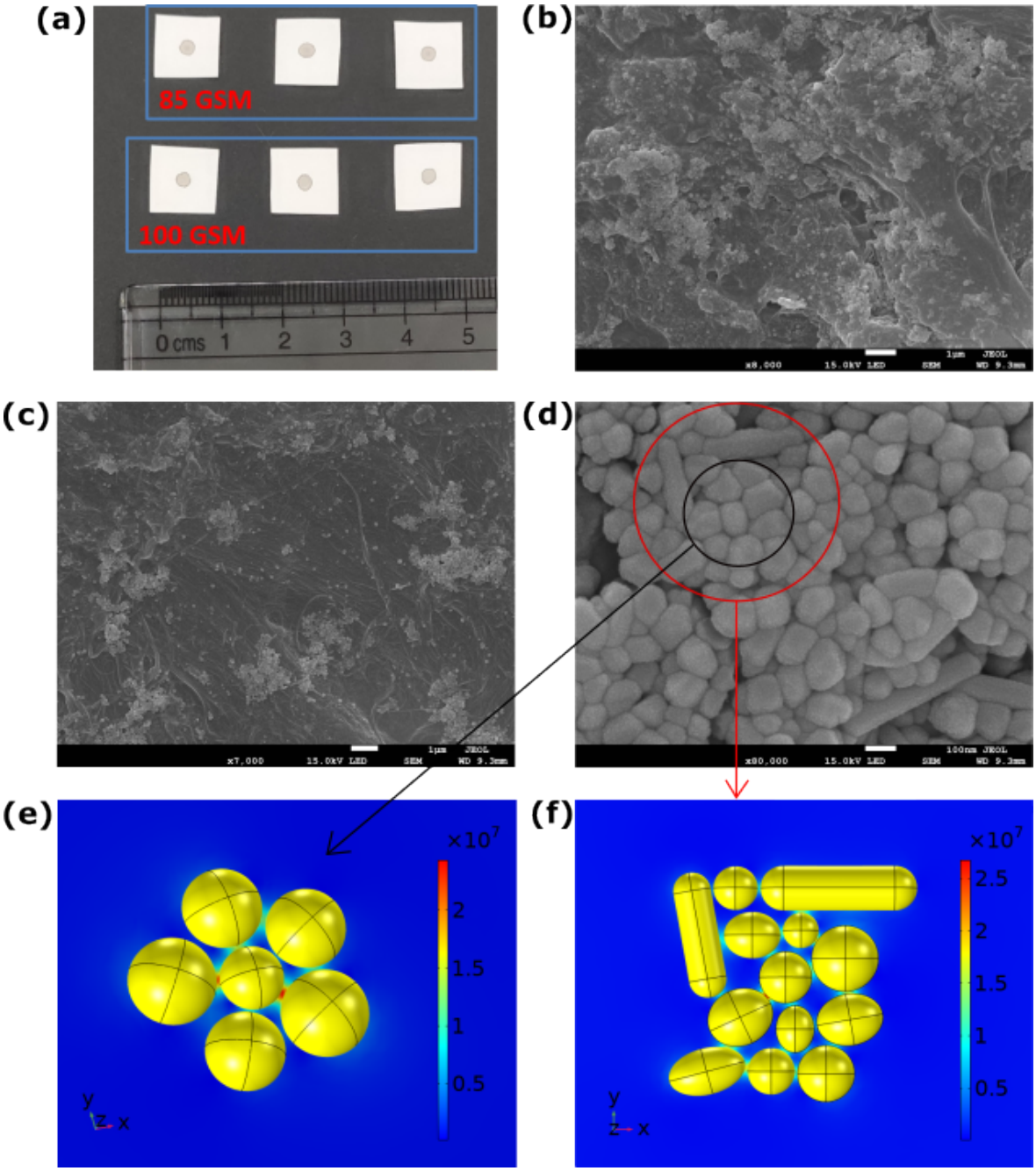

Figure 6.3: (a) Images of AgNP decorated 85 GSM and 100 GSM paper SERS substrates having grey circular spots as sensing regions. FESEM image showing the distribution of AgNPs over the (b) 85 GSM and (c) 100 GSM paper SERS substrates. (d) Zoomed image of one AgNP cluster on the 85 GSM paper SERS substrate. Local electric field generation due to different distributions of AgNPs, (e) 5 AgNPs of diameter 100 nm and one AgNP of diameter 80 nm at the center of the arrangement, and (f) the random distribution of AgNPs taken from the FESEM image.

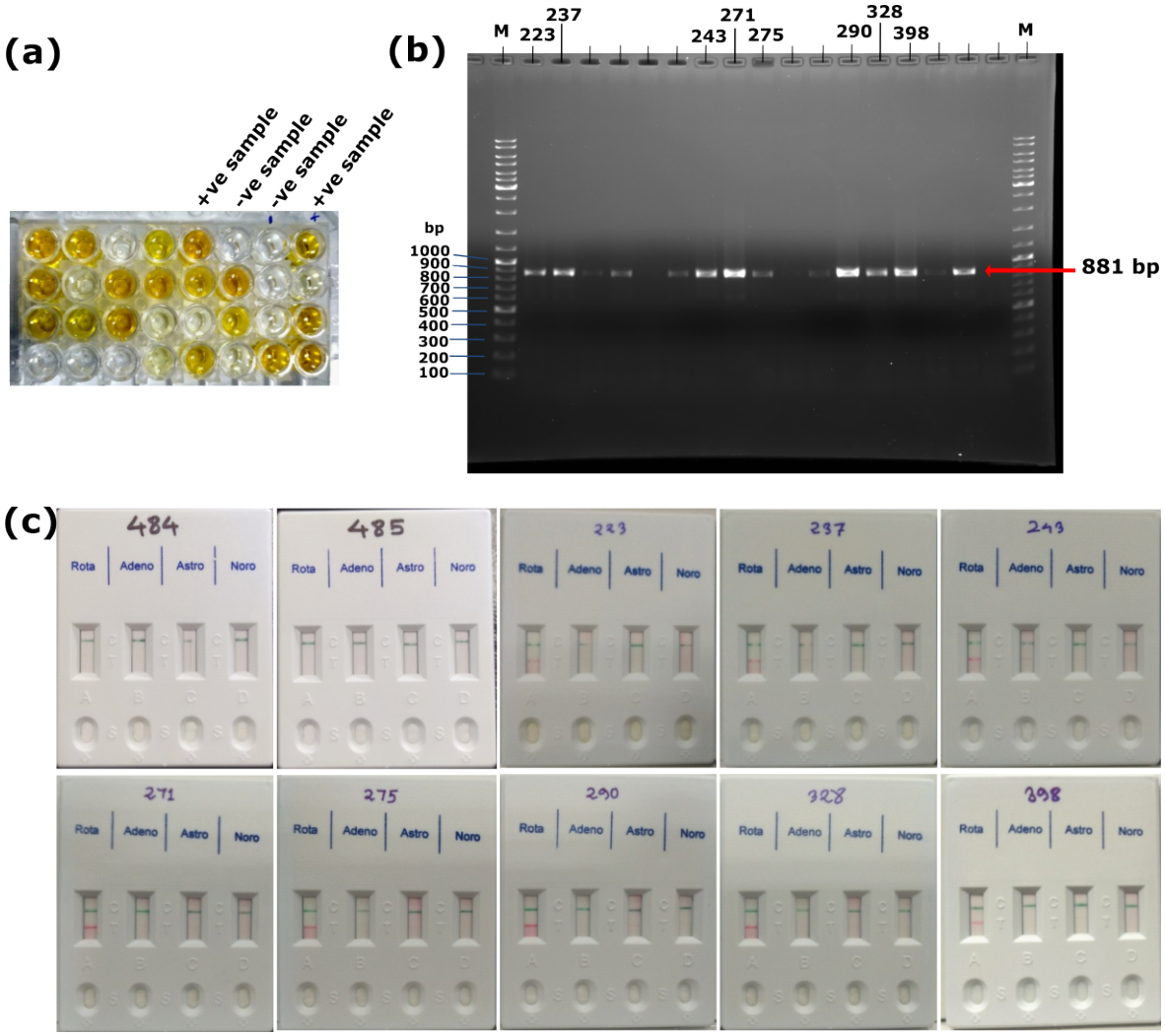

Figure 6.4: (a) Detection of rotavirus by ELISA using Premier® Rotaclone® kit from Meridian Bioscience, Inc., (b) Confirmation of the presence of rotavirus by PCR, (c) Confirmation of Control samples and Rotavirus samples from clinical stool samples using CerTest Rota + Astro + Noro + Adeno rapid antigen test (CerTest Biotech).

on the principle of a qualitative ICA has also been performed for the determination of rotavirus, adenovirus, astrovirus, and norovirus (genogroup I and II) in the stool samples. In this colorimetric technique as depicted in figure 6.4(c), the red line in the test line indicates the presence of the virus and the green line indicates the control line. Anti-rotavirus antibodies, anti-adenovirus antibodies, anti-astrovirus antibodies, and anti-norovirus antibodies that are present on the membranes of strip A (test line), strip B (test line), strip C (test line), and strip D (test line), respectively, capture the coloured conjugate and a red line appears in the strips. The detail on rotavirus isolates acquired from clinical diarrhoea stool samples has been provided in Table 6.1.

Table 6.1: Details of rotavirus isolates from clinical diarrhea stool samples

Sl. No.	Sample No.	Isolate No.	Date of isolation	Place of isolation	Genotype (Rotavirus)	ELISA result for Rotavirus (Score cut off= 0.150	CerTest Rota+Astro+ Noro+Adeno rapid antigen test	Verified by PCR	Verified by RNA PAGE
1	484	RM6072018	30-07-2018	RIMS, Imphal	-	Negative(0.1011)	Negative for all	Yes	Yes
2	485	RM35122018	27-12-2018	RIMS, Imphal	-	Negative(0.105)	Negative for all	Yes	Yes
3	223	RM193062016	22-11-2016	RIMS, Imphal	G3Pnt	Positive (2.746)	Positive for Rotavirus	Yes	Yes
4	237	RM315052017	02-05-2017	RIMS, Imphal	G3Pnt	Positive (2.6115)	Positive for Rotavirus	Yes	Yes
5	290	RM275022017	03-02-2017	RIMS, Imphal	G3Pnt	Positive (>3.5)	Positive for Rotavirus	Yes	Yes
6	243	RM298032017	30-03-2017	RIMS, Imphal	G2Pnt	Positive (2.4937)	Positive for Rotavirus	Yes	Yes
7	271	RM314052017	17-05-2017	RIMS, Imphal	G3Pnt	Positive (>3.5)	Positive for Rotavirus	Yes	Yes
8	275	RM222112016	14-11-2016	RIMS, Imphal	G3Pnt	Positive (>3.5)	Positive for Rotavirus	Yes	Yes
9	328	RM265012017	10-01-2017	RIMS, Imphal	G3Pnt	Positive (>3.5)	Positive for Rotavirus	Yes	Yes
10	398	RM386012018	29-01-2018	RIMS, Imphal	G3Pnt	Positive (0.5243)	Positive for Rotavirus	Yes	Yes

6.3 Results and discussions

6.3.1 SERS performance of the fabricated substrate

Raman spectral signatures of the standard Raman active samples were initially analyzed to evaluate the performance of the developed SERS substrate. 1 µM solutions of MG and R6G have been prepared and each sample of volume 10 µL has been pipetted on two 85 GSM paper SERS substrates. Figure 6.5(a) and 6.5(b) represent the SERS spectra of MG and R6G collected from 10 different points on the sensing region of the substrate. The average spectrum has been represented in a dark line for both samples. The characteristic peaks of MG at 796 cm^{-1}, 1172 cm^{-1}, 1216 cm^{-1}, 1390 cm^{-1}, and 1614 cm^{-1} are attributed to ring C-H out-of-plane bending, ring C-H in-plane vibration, C-H rocking, N-phenyl stretching and ring C-C in-plane stretching vibrations [28–30], respectively. The Raman peaks of R6G at 614 cm^{-1}, 770 cm^{-1}, 1126 cm^{-1}, and 1310 cm^{-1} are attributed to C-C-C in-plane bending, C-H out-of-plane bending, C-H in-plane bending, C=C stretching vibrations, respectively [31]. The vibrational peak at 1182 cm^{-1} is attributed to C-H and N-H bending vibrations [31]. The peaks at 1362 cm^{-1}, 1510 cm^{-1}, and 1650 cm^{-1} are attributed to C-C stretching vibration [32]. From figure 6.5(a) and 6.5(b), the signal intensity fluctuations for MG and R6G were estimated to be below 8% for both samples. Clearly, the characteristic spectra suggest that the proposed SERS substrate yields a fairly stable and reproducible signal for the standard Raman active sample. These low values of intensity fluctuations suggest that the proposed SERS substrate has a good degree of reproducibility characteristics.

The average EF (EF_{avg}) of the developed SERS substrate has been estimated using the following equation as discussed in the section 1.3.3:

$$EF_{avg} = \frac{\frac{I_{SERS}}{N_{SERS}}}{\frac{I_{Raman}}{N_{Raman}}} \tag{6.1}$$

To estimate the EF_{avg}, 10 µL of MG of concentration 10 mM was pipetted on a plane 85 GSM paper substrate and dried in a vacuum desiccator for 1 hour. Raman spectra of MG from different points of the plane paper substrate were recorded and the average peak intensity corresponding to the peak 1172 cm^{-1} was found to be 650 a.u. Similarly, 10 µL MG of concentration 1 nM was pipetted on the sensing region of the proposed 85 GSM paper SERS substrate, and subsequently, upon drying, Raman spectra were collected. The average Raman signal intensity for 1172 cm^{-1} peak has been estimated to be 350 a.u. From equation 6.1, the EF_{avg} of the designed substrate is calculated to be 5×10^6. Figure 6.5(c) represents the variation of Raman intensity with different concentrations of MG from 2 µM to 20 nM collected from 85 GSM paper SERS substrate. MG concentration as low as 50 nM could be easily detected using the fabricated 85 GSM paper SERS substrates. The SERS signal intensities of MG

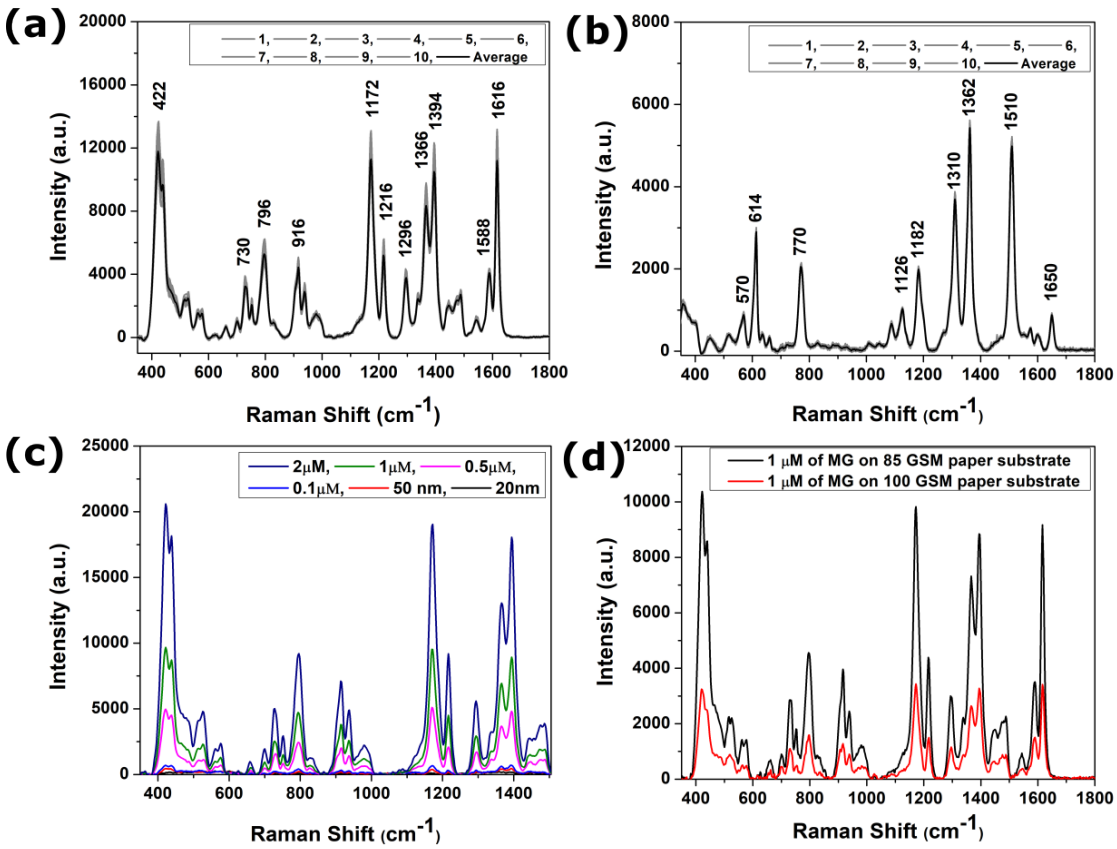

Figure 6.5: SERS spectra of (a) MG and (b) R6G of concentration 1 µM collected from 85 GSM paper SERS substrates. Each figure contains the SERS spectrum from 10 different points and their average spectrum. (c) Variation of Raman signal intensity with the concentration of MG from 2 µM to 20 nM collected from 85 GSM paper SERS substrate. (d) SERS signal intensities of 1 µM of MG collected from 85 and 100 GSM paper SERS substrates.

molecules were recorded from 100 GSM paper SERS substrates. Figure 6.5(d) shows the SERS signal intensities of 1 µM MG scattered from 85 and 100 GSM grade paper SERS substrates. Clearly, as compared to 100 GSM paper, with 85 GSM grade paper, the fabricated SERS substrate yields a significant enhancement in the scattered Raman signals for the considered sample, attributed to more uniform AgNPs distribution in the micropores of the 85 GSM paper substrate as compared to 100 GSM paper substrate. This has been evident from the captured FESEM images for these two different GSM grade papers shown in figure 6.3(b) and 6.3(c). Although a fairly modest EF_{avg} has been observed with the 85 GSM paper SERS substrate, the rapid and relatively simpler steps involved in the fabrication of the present SERS substrate provides an edge over the SERS substrates reported elsewhere [33, 34].

Next, 10 different pieces of 85 GSM grade paper SERS substrates have been treated with 10 µL volume of 1 µM of MG. From the figure 6.6(a), the RSD values of Raman signal intensity collected from the indivisual SERS substrates for the peak 1172 cm^{-1} are found to be within 9%. On the other hand, variation of the average SERS signal intensities form the 10 substrates has been calculated to be 10%, which suggests a good degree of reproducibility of different batches of SERS substrates.

The limit of detection (LoD) has been evaluated using the 85 GSM paper SERS substrates treated with 5 different concentrations of MG. Scattered Raman signals from 5 different points on the substrates are collected. Figure 6.6(b) represents the normalized SERS signal intensity variations with different concentrations of MG for the peak at 1172 cm^{-1}. LoD of the fabricated SERS substrate has been estimated using the standard equation:

$$LoD = \frac{3\sigma}{S}, \tag{6.2}$$

where, σ and S represent the standard deviation of y-intercepts and the slope of the linear fitted line, respectively. From equation 6.2, the LoD of MG is calculated to be 22 nM.

Next, Raman signal intensity variation with aging time of the fabricated SERS substrates have been studied. 20 pieces of 85 GSM paper-based SERS substrates have been prepared following the procedure mentioned earlier, and kept in a vaccum desiccator. Next, on each consecutive days, one of these substrates were treated with 1 µM of MG of volume 10 µL, and dried for 1 hour before collecting the Raman spectra. Figure 6.6(c) displays the Raman intensity for the peak 1172 cm^{-1} of MG collected for 20 consecutive days. For the first 15 days, the signal intensity is found acceptably stable. However, beyond this period it started to degrade suggesting that the proposed SERS substrate can be best used within 2 weeks from the day of fabrication of the substrate.

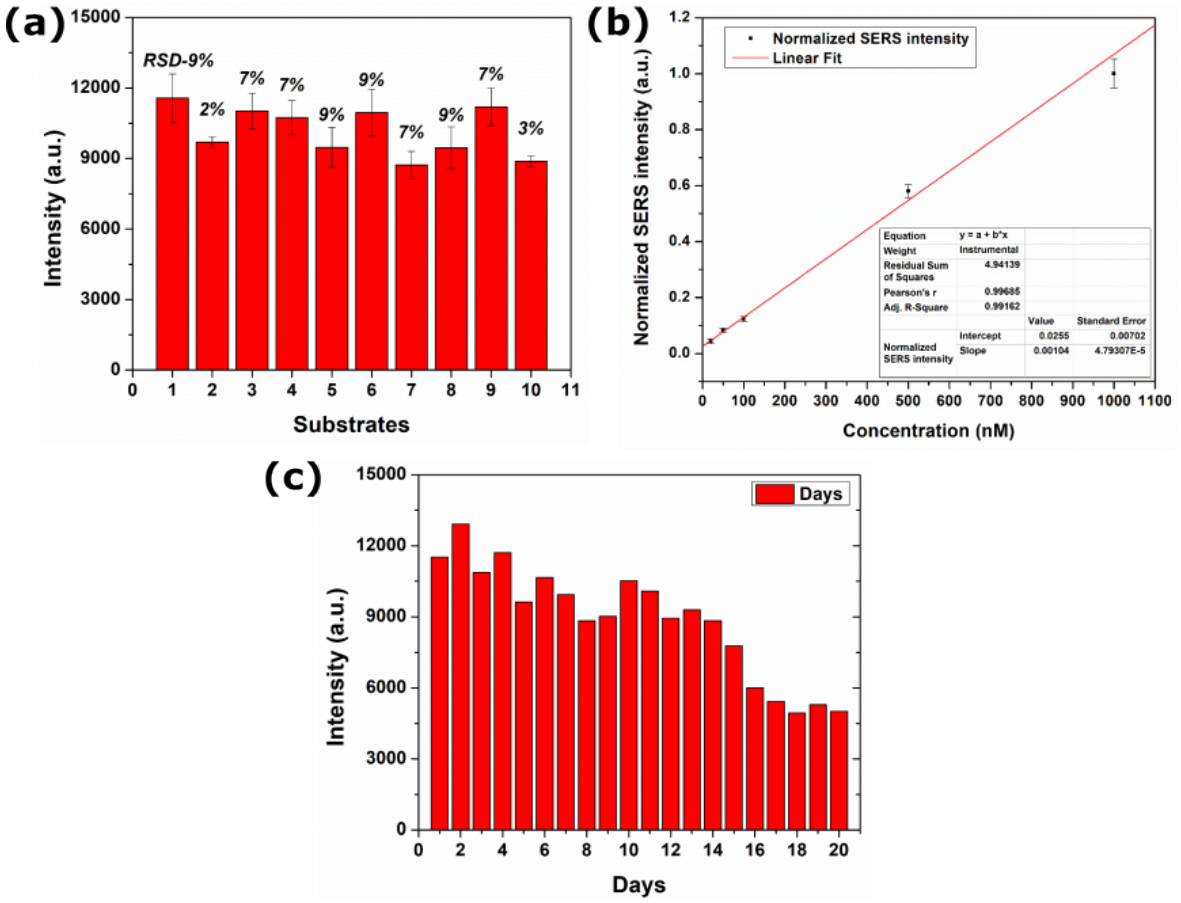

Figure 6.6: (a) Histogram plot of Raman intensity of 1 µM of MG at 1172 cm^{-1} collected from 10 different substrates. (b) Variation of SERS intensity with different concentrations of MG for the peak at 1172 cm^{-1}. (c) Variation of SERS signal intensity with aging time of the 85 GSM paper SERS substrates.

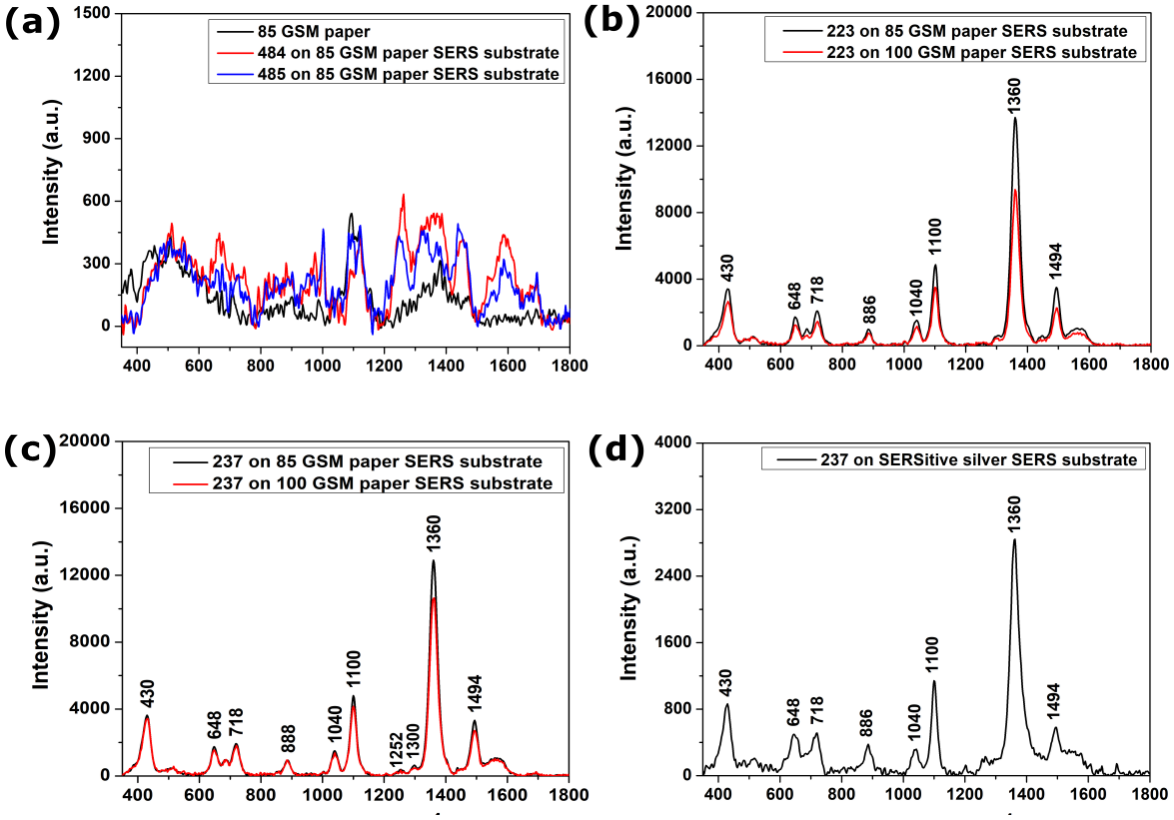

Figure 6.7: (a) Raman spectra of 85 GSM paper and SERS spectra of control samples 484 and 485 collected from 85 GSM paper SERS substrates. SERS spectra of rotavirus samples (b) 223 and (c) 237 collected from 85 GSM and 100 GSM paper SERS substrates. (d) SERS spectrum of rotavirus sample 237 collected from the commercial SERSitive silver SERS substrate.

6.3.2 SERS spectra of rotavirus particles in solution

Prior to the detection of the rotavirus particles with the proposed SERS substrates, Raman spectrum investigation was carried out for the control samples. Samples 484 and 485 in the Table 6.1 are the control samples. Figure 6.7(a) indicates the recorded Raman spectra of bare 85 GSM paper substrate, samples 484 and 485 from the 85 GSM paper SERS substrates. The figure clearly indicates that no significant SERS spectra of the control sample have been noticed for the bare paper substrate.

Following this observation, Raman signal analysis of positive samples was performed on different GSM grade paper SERS substrates. Figure 6.7(b) and 6.7(c) illustrate the characteristic Raman peaks of two such positive samples namely 223 and 237 when the scattered Raman signals were recorded from 85 GSM and 100 GSM paper substrates. Here also, it has been observed that with 85 GSM paper substrate, the SERS signal intensity of rotavirus samples is more enhanced than the 100 GSM grade paper substrate. The characteristic Raman peaks at 648 cm^{-1} and 685 cm^{-1} are attributed to tyrosine C-C twist [16] and cysteine C-H stretching vibration [35], respectively. Further, the tryptophan indole ring vibration is responsible for the Raman peaks at 886 cm^{-1} and

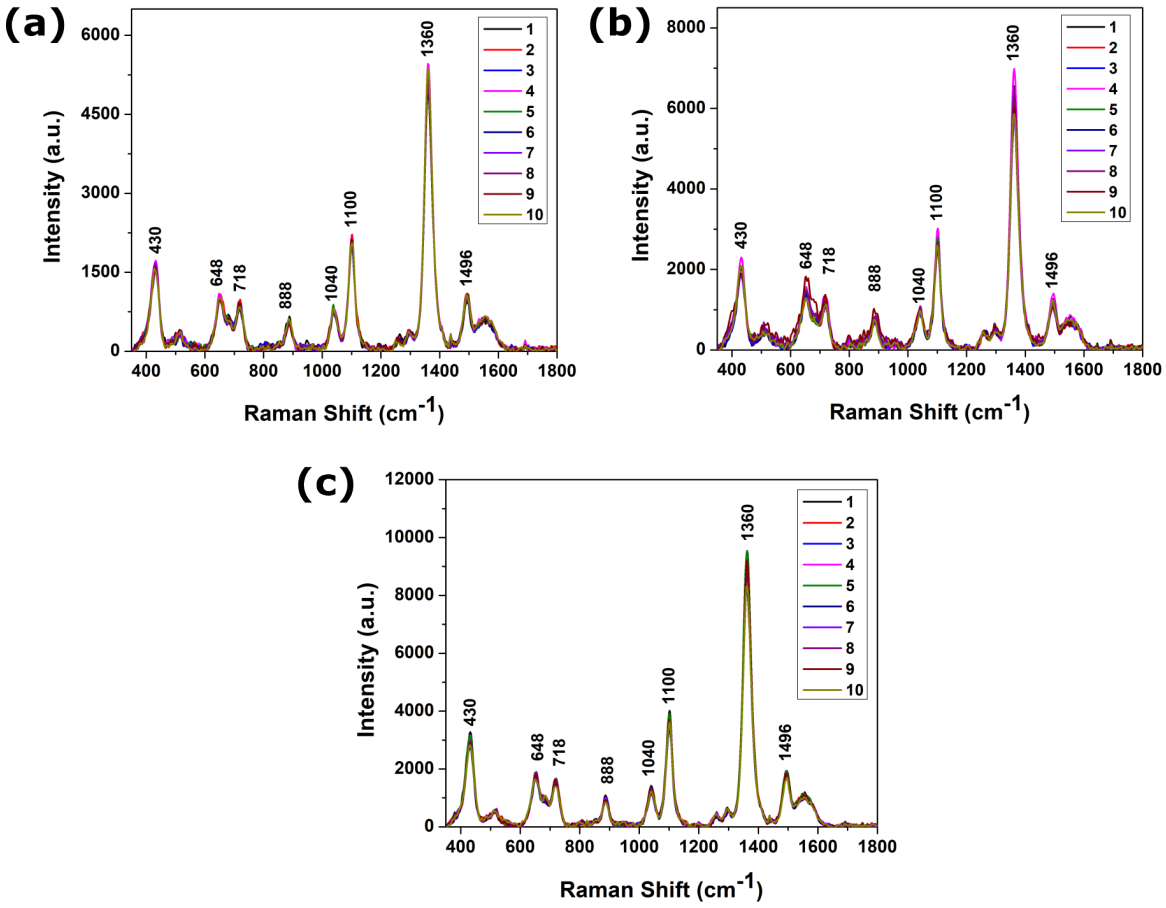

Figure 6.8: SERS spectra of rotavirus sample 290 of concentrations (a) 10%, (b) 20% and (c) 30% collected using 85 GSM paper-based SERS substrate.

1360 cm^{-1} [36]. Again in figure 6.7(b) and 6.7(c), Raman peak shift of 2 cm^{-1} that corresponds to the peak position 886 cm^{-1} has been observed with two different clinical stool samples. The peaks at 718 cm^{-1} and 1100 cm^{-1} are attributed to the ring breathing mode of adenine and the O-P-O backbone stretching of the nucleic acid present in the stool sample [35], respectively. Due to the vibration of phenylalanine symmetric ring breathing mode [26] and C-H in-plane bending mode [35], signature Raman peaks can be found at 1003 cm^{-1} and 1040 cm^{-1}, respectively. The strong Raman peak at 430 cm^{-1} is emerging because of the torsion vibration of the NH_2 group [37]. Two characteristic peaks for deoxycytidine triphosphate are found at 1252 cm^{-1} and 1300 cm^{-1} in the SERS spectra of the rotavirus samples [38].

Next, three 85 GSM paper SERS substrates are considered and treated with 10 µL volume of rotavirus sample 290 of concentrations 10%, 20% and 30%, respectively. The Raman spectra from 10 different points are collected after 1 hour of drying in vacuum desiccator. Figure 6.8(a-c) represent SERS spectra of three concentrations of the rotavirus sample. The relative standard deviation (RSD) values of the Raman signal intensity corresponding to the peak position 1362 cm^{-1} are estimated to be 3%,

6% and 5% for the concentrations 10%, 20% and 30%, respectively.

6.3.3 SERS spectra of rotavirus particles collected from the SERSitive SERS substrate

In order to validate the Raman signal analysis obtained from the proposed paper-based SERS substrate, SERS signal of the same rotavirus sample was recorded from a commercial-grade SERS substrate. Commercially available SERS substrates from SERSitive Inc. (https://sersitive.eu/) have been considered in this present work. Figure 6.7(d) depicts the characteristic peaks of the rotavirus sample 237 when the scattered signal was recorded from this SERS substrate. The Raman peak positions of the rotavirus samples collected using the commercial and the proposed paper-based SERS substrates are found to be similar which again infers the viability of the proposed sensing scheme for such purpose.

Furthermore, the used paper-based SERS substrates can be disposed by dipping the paper into a solution containing detergents (like triton X-100) for 5 to 10 minutes as the detergent molecules are known to cause disintegration of many virus particles including rotavirus.

6.4 Summary

In summary, a relatively simpler and rapid SERS substrate fabrication technique has been proposed to detect rotavirus in clinical stool samples. The designed substrates have been obtained by drop-casting of AgNPs on different GSM-grade papers. The experimental data obtained from the paper-based SERS substrate has been compared with the data from a commercial-grade counterpart and a fairly accurate results yielded by the proposed scheme has been noticed. Owing to its low-fabrication cost INR 5 ($\sim$ \$0.06) per substrate, the fabricated substrates can be used as disposable and for large-scale sensing of rotavirus particles.

Bibliography

[1] Lestari, F. B., Vongpunsawad, S., Wanlapakorn, N., and Poovorawan, Y. Rotavirus infection in children in southeast asia 2008–2018: disease burden, genotype distribution, seasonality, and vaccination. *Journal of biomedical science*, 27:1–19, 2020.

[2] Crawford, S. E., Ramani, S., Tate, J. E., Parashar, U. D., Svensson, L., Hagbom,

M., Franco, M. A., Greenberg, H. B., O'Ryan, M., Kang, G., et al. Rotavirus infection. *Nature Reviews Disease Primers*, 3(1):1–16, 2017.

[3] Sadiq, A., Bostan, N., Yinda, K. C., Naseem, S., and Sattar, S. Rotavirus: Genetics, pathogenesis and vaccine advances. *Reviews in medical virology*, 28(6):e2003, 2018.

[4] Kawai, K., O'Brien, M. A., Goveia, M. G., Mast, T. C., and El Khoury, A. C. Burden of rotavirus gastroenteritis and distribution of rotavirus strains in asia: a systematic review. *Vaccine*, 30(7):1244–1254, 2012.

[5] Uprety, T., Sreenivasan, C. C., Hause, B. M., Li, G., Odemuyiwa, S. O., Locke, S., Morgan, J., Zeng, L., Gilsenan, W. F., Slovis, N., et al. Identification of a ruminant origin group b rotavirus associated with diarrhea outbreaks in foals. *Viruses*, 13(7):1330, 2021.

[6] Devi, Y. D., Devi, A., Gogoi, H., Dehingia, B., Doley, R., Buragohain, A. K., Singh, C. S., Borah, P. P., Rao, C. D., Ray, P., et al. Exploring rotavirus proteome to identify potential b-and t-cell epitope using computational immunoinformatics. *Heliyon*, 6(12), 2020.

[7] Anaya-Molina, Y., Hernández, S. I. D. L. C., Andrés-Dionicio, A. E., Terán-Vega, H. L., Méndez-Pérez, H., Castro-Escarpulli, G., and García-Lozano, H. A one-step real-time rt-pcr helps to identify mixed rotavirus infections in mexico. *Diagnostic microbiology and infectious disease*, 92(4):288–293, 2018.

[8] Joshi, M. S., Deore, S. G., Walimbe, A. M., Ranshing, S. S., and Chitambar, S. D. Evaluation of different genomic regions of rotavirus a for development of real time pcr. *Journal of virological methods*, 266:65–71, 2019.

[9] Memon, A. M., Bhuyan, A. A., Chen, F., Guo, X., Menghwar, H., Zhu, Y., Ku, X., Chen, S., Li, Z., and He, Q. Development and validation of monoclonal antibody-based antigen capture elisa for detection of group a porcine rotavirus. *Viral immunology*, 30(4):264–270, 2017.

[10] Rippa, M., Castagna, R., Brandi, S., Fusco, G., Monini, M., Chen, D., Zhou, J., Zyss, J., and Petti, L. Octupolar plasmonic nanosensor based on ordered arrays of triangular au nanopillars for selective rotavirus detection. *ACS Applied Nano Materials*, 3(5):4837–4844, 2020.

[11] Pineda, M. F., Chan, L. L.-Y., Kuhlenschmidt, T., Choi, C. J., Kuhlenschmidt, M., and Cunningham, B. T. Rapid specific and label-free detection of porcine rotavirus using photonic crystal biosensors. *IEEE Sensors Journal*, 9(4):470–477, 2009.

[12] Li, Z., Zhao, F., Tang, T., Wang, M., Yu, X., Wang, R., Li, Y., Xu, Y., Tang, L., Wang, L., et al. Development of a colloidal gold immunochromatographic strip assay for rapid detection of bovine rotavirus. *Viral Immunology*, 32(9):393–401, 2019.

[13] Chen, H., Park, S.-G., Choi, N., Moon, J.-I., Dang, H., Das, A., Lee, S., Kim, D.-G., Chen, L., and Choo, J. Sers imaging-based aptasensor for ultrasensitive and reproducible detection of influenza virus a. *Biosensors and Bioelectronics*, 167:112496, 2020.

[14] Chen, H., Park, S.-G., Choi, N., Kwon, H.-J., Kang, T., Lee, M.-K., and Choo, J. Sensitive detection of sars-cov-2 using a sers-based aptasensor. *Acs Sensors*, 6(6): 2378–2385, 2021.

[15] Liu, M., Zheng, C., Cui, M., Zhang, X., Yang, D.-P., Wang, X., and Cui, D. Graphene oxide wrapped with gold nanorods as a tag in a sers based immunoassay for the hepatitis b surface antigen. *Microchimica Acta*, 185:1–8, 2018.

[16] Yadav, S., Senapati, S., Desai, D., Gahlaut, S., Kulkarni, S., and Singh, J. Portable and sensitive ag nanorods based sers platform for rapid hiv-1 detection and tropism determination. *Colloids and Surfaces B: Biointerfaces*, 198:111477, 2021.

[17] Driskell, J. D., Zhu, Y., Kirkwood, C. D., Zhao, Y., Dluhy, R. A., and Tripp, R. A. Rapid and sensitive detection of rotavirus molecular signatures using surface enhanced raman spectroscopy. *PloS one*, 5(4):e10222, 2010.

[18] Fan, Z., Yust, B., Nellore, B. P. V., Sinha, S. S., Kanchanapally, R., Crouch, R. A., Pramanik, A., Chavva, S. R., Sardar, D., and Ray, P. C. Accurate identification and selective removal of rotavirus using a plasmonic–magnetic 3d graphene oxide architecture. *The Journal of Physical Chemistry Letters*, 5(18):3216–3221, 2014.

[19] Zhang, Y., Wu, G., Wei, J., Ding, Y., Wei, Y., Liu, Q., and Chen, H. Rapid and sensitive detection of rotavirus by surface-enhanced raman scattering immunochromatography. *Microchimica Acta*, 188:1–10, 2021.

[20] Sarma, D., Biswas, S., Hatiboruah, D., Chamuah, N., and Nath, P. 100 gsm paper as an sers substrate for trace detection of pharmaceutical drugs in an aqueous medium. *Journal of Physics D: Applied Physics*, 55(38):385102, 2022.

[21] Chamuah, N., Hazarika, A., Hatiboruah, D., and Nath, P. Sers on paper: an extremely low cost technique to measure raman signal. *Journal of Physics D: Applied Physics*, 50(48):485601, 2017.

[22] Zhang, K., Zhao, J., Xu, H., Li, Y., Ji, J., and Liu, B. Multifunctional paper strip based on self-assembled interfacial plasmonic nanoparticle arrays for sensitive sers detection. *ACS applied materials & interfaces*, 7(30):16767–16774, 2015.

[23] Godoy, N., García-Lojo, D., Sigoli, F., Pérez-Juste, J., Pastoriza-Santos, I., and Mazali, I. Ultrasensitive inkjet-printed based sers sensor combining a high-performance gold nanosphere ink and hydrophobic paper. *Sensors and Actuators B: Chemical*, 320:128412, 2020.

[24] Hu, S.-W., Qiao, S., Pan, J.-B., Kang, B., Xu, J.-J., and Chen, H.-Y. A paper-based sers test strip for quantitative detection of mucin-1 in whole blood. *Talanta*, 179:9–14, 2018.

[25] Song, J. Y. and Kim, B. S. Rapid biological synthesis of silver nanoparticles using plant leaf extracts. *Bioprocess and biosystems engineering*, 32:79–84, 2009.

[26] Biswas, S., Devi, Y. D., Sarma, D., Namsa, N. D., and Nath, P. Gold nanoparticle decorated blu-ray digital versatile disc as a highly reproducible surface-enhanced raman scattering substrate for detection and analysis of rotavirus rna in laboratory environment. *Journal of Biophotonics*, 15(11):e202200138, 2022.

[27] Devi, Y. D., Dey, U., Kumar, A., Singh, C. S., and Namsa, N. D. Genome sequence of a wa-like g3p [8] rotavirus from a 12-month-old child with diarrhea in manipur, india. *Microbiology Resource Announcements*, 11(8):e01254–21, 2022.

[28] Kumar, P., Khosla, R., Soni, M., Deva, D., and Sharma, S. K. A highly sensitive, flexible sers sensor for malachite green detection based on ag decorated microstructured pdms substrate fabricated from taro leaf as template. *Sensors and Actuators B: Chemical*, 246:477–486, 2017.

[29] Pu, H., Zhu, H., Xu, F., and Sun, D.-W. Development of core-satellite-shell structured mnp@ au@ mil-100 (fe) substrates for surface-enhanced raman spectroscopy and their applications in trace level determination of malachite green in prawn. *Journal of Raman Spectroscopy*, 53(4):682–693, 2022.

[30] He, L., Kim, N.-J., Li, H., Hu, Z., and Lin, M. Use of a fractal-like gold nanostructure in surface-enhanced raman spectroscopy for detection of selected food contaminants. *Journal of agricultural and food chemistry*, 56(21):9843–9847, 2008.

[31] Wang, Y. Q., Ma, S., Yang, Q. Q., and Li, X. J. Size-dependent sers detection of r6g by silver nanoparticles immersion-plated on silicon nanoporous pillar array. *Applied surface science*, 258(15):5881–5885, 2012.

[32] Wu, W., Liu, L., Dai, Z., Liu, J., Yang, S., Zhou, L., Xiao, X., Jiang, C., and Roy, V. A. Low-cost, disposable, flexible and highly reproducible screen printed sers substrates for the detection of various chemicals. *Scientific reports*, 5(1):10208, 2015.

[33] Yang, G., Fang, X., Jia, Q., Gu, H., Li, Y., Han, C., and Qu, L.-L. Fabrication of paper-based sers substrates by spraying silver and gold nanoparticles for sers determination of malachite green, methylene blue, and crystal violet in fish. *Microchimica Acta*, 187:1–10, 2020.

[34] Feng, L., Duan, J., Wang, K., Huang, L., and Xiao, G. Efficient fabrication of highly sensitive agnps-drawing paper sers substrates by robotic writing approach. *Spectrochimica Acta Part A: Molecular and Biomolecular Spectroscopy*, 261:120064, 2021.

[35] Ochsenkuhn, M. A., Jess, P. R., Stoquert, H., Dholakia, K., and Campbell, C. J. Nanoshells for surface-enhanced raman spectroscopy in eukaryotic cells: cellular response and sensor development. *Acs Nano*, 3(11):3613–3621, 2009.

[36] Miura, T., Takeuchi, H., and Harada, I. Characterization of individual tryptophan side chains in proteins using raman spectroscopy and hydrogen-deuterium exchange kinetics. *Biochemistry*, 27(1):88–94, 1988.

[37] Singh, J. Laser raman and infra-red spectra of biomolecule: 5-aminouracil. *Pramana*, 70:479–486, 2008.

[38] Pezzotti, G., Horiguchi, S., Boschetto, F., Adachi, T., Marin, E., Zhu, W., Yamamoto, T., Kanamura, N., Ohgitani, E., and Mazda, O. Raman imaging of individual membrane lipids and deoxynucleoside triphosphates in living neuronal cells during neurite outgrowth. *ACS chemical neuroscience*, 9(12):3038–3048, 2018.